Journal of Materials Chemistry A

Evaluation procedure of photocatalysts for VOCs degradation from the view of density functional theory calculations: g-C3N4 dots/graphene as an example

Journal:	*Journal of Materials Chemistry A*
Manuscript ID	TA-ART-06-2020-006060.R1
Article Type:	Paper
Date Submitted by the Author:	26-Jul-2020
Complete List of Authors:	Jing, Binghua; Guangdong University of Technology Ao, Zhimin; Guangdong University of Technology, School of Environmental Science and Engineering Zhao, Weina; Guangdong University of Technology, School of Environmental Science and Engineering Xu, Ying; Hunan University of Science and Technology Chen, Zhongfang; University of Puerto Rico, Department of Chemistry An, Taicheng; Guangdong University of Technology, Institute of Environmental Health and Pollution Control

ARTICLE

Evaluation procedure of photocatalysts for VOCs degradation from the view of density functional theory calculations: g-C_3N_4 dots/graphene as an example

Received 00th January 20xx,
Accepted 00th January 20xx

DOI: 10.1039/x0xx00000x

Binghua Jing, [a] Zhimin Ao, *[a] Weina Zhao, [a] Ying Xu, [b] Zhongfang Chen, [c] and Taicheng An [a]

Various techniques have been utilized in experiments to evaluate the performance of photocatalysts and understand the corresponding catalytic mechanism. However, it is still challenging to demonstrate the phenomenon in detailed during the catalytic process in experiments to fundamentally understand the catalytic mechanism. Density function theory (DFT) is an excellent technique to solve this problem in the level of electrons and atoms. However, the evaluation procedure of photocatalysts based on DFT calculations was unclear. Thus, in this work, we propose the evaluation procedure of photocatalysts for volatile organic compounds (VOCs) degradation from the view of DFT calculations through following aspects: (i) band structure of photocatalysts, including the band gap, the capability of photo adsorption and the positions of conduction band (CB) and valence band (VB); (ii) adsorption of H_2O, O_2 or other oxidants; (iii) adsorption of pollutants; (iv) reaction pathway for pollutant degradation. To demonstrate the application of the proposed evaluation procedure, g-C_3N_4 dots/graphene is taken as an example to evaluate the photocatalytic performance. Results show that the g-C_3N_4 dots/graphene has an enhanced visible light absorption with significantly reduced height for photoelectron excitation and the photoelectron immigrates between the heterostructure, from the valence band of g-C_3N_4 dots to graphene layer, and then to the conduction band of g-C_3N_4 dots, which promotes light adsorption and induces the generation of electron-hole pairs with low recombination rate. In addition, both the adsorbed H_2O and O_2 have strong interaction with g-C_3N_4 dots/graphene, inducing the activation to form ·OH and $\cdot O_2^-$ radicals to attack and degrade the adsorbed VOCs. Therefore, procedure to evaluate performance of photocatalyst for VOCs degradation based on DFT calculations is proposed in this work, and the evaluation procedure is successfully applied to predict the high photocatalytic performance of g-C_3N_4 dots/graphene, where unique photoelectron excitation pathway is also demonstrated between the heterostructure.

1. Introduction

Volatile organic compounds (VOCs) are one type of main air pollutants,[1-4] and have adverse effect on atmosphere environment and health of human and animals.[5] For example, VOCs are the precursors for some environmental hazards, such as photochemical fumes, haze, pinkeye[6, 7] and so on. Therefore, the release of VOCs should be strictly controlled.[2] Photocatalytic degradation of VOCs is one of promising techniques for controlling VOCs emission.[8] Importantly, photocatalyst is critical for this technique.[9]

To develop high performance photocatalysts and understand the corresponding catalytic mechanism, various techniques have been utilized in experiment.[10-13] For example, X-ray photoelectron spectroscope (XPS) can be used to detect the elemental composition of photocatalysts, Brunauer-Emmett-Teller (BET) can evaluate the specific surface area and pore size distribution of photocatalysts, Electron paramagnetic resonance (EPR) is applied to probe the reactive radicals generated, and photoluminescence (PL) is carried out to reveal the migration, transfer and recombination processes of electron-hole pairs. Although above experimental techniques can test the photocatalytic performance directly, and the catalysis mechanism can be also interpreted correspondingly, it is challenging to demonstrate the process in the electronic and atomic level, and fundamentally understand the photocatalytic mechanism. However, the corresponding information can be directly provided by density functional theory (DFT) calculations.[14] The self-consistent calculation determinates the active photocatalytic site and atomic structure of gas molecule on the active site;[15] band structure and Highest Occupied Molecular Orbital – Lowest Unoccupied Molecular Orbital (HOMO-LUMO) can be used to estimate electron-hole pairs generation and recombination pathway;[16] transition state search (TS) conformation is an excellent method to demonstrate the reaction pathway.[17]

[a] Guangdong Key Laboratory of Environmental Catalysis and Health Risk Control, Guangzhou Key Laboratory Environ-mental Catalysis and Pollution Control, School of Environmental Science and Engineering, Institute of Environmental Health and Pollution Control, Guangdong University of Technology, Guangzhou 510006, China. E-mail address: zhimin.ao@gdut.edu.cn.
[b] School of Physics and Electronic Science, Hunan University of Science and Technology, Xiangtan 411201, China.
[c] Department of Chemistry, University of Puerto Rico, Rio Piedras, San Juan, PR 00931, USA.

† Electronic Supplementary Information (ESI) available: [details of any supplementary information available should be included here]. See DOI: 10.1039/x0xx00000x

However, the evaluation procedure of the performance of photocatalytic pollutant degradation based on DFT calculations was not yet systematically studied. It is known that the main photocatalytic activity is originally from the photo excited electrons and holes, which can react with H_2O and O_2 molecules or other oxidants to generate reactive oxidation species (ROSs), such as ·OH and $\cdot O_2^-$. The generated ROSs attack organic bonds in organic pollutants, which are finally mineralized into CO_2 and H_2O.[11, 18] Therefore, the effective generation of electrons–hole pairs and their utilization are the key factors. In addition, electrons in semiconductors can be exited from valence band (VB) to conduction band (CB) when the energy of light irradiation is higher than the band gap of semiconductor,[19, 20] generating free electrons in CB while leaving holes in VB. However, the generated electrons and holes may be quickly recombined if they cannot be separated or utilized promptly.[13] Furthermore, the positions of VB and CB determine the oxidative and reductive capability of photocatalysts, i.e. the capability of utilization of the generated electrons and holes to produce ROSs. Therefore, the band structure of semiconductors, including the band gap and the positions of CB and VB, is another key factor. On the other hand, the adsorption of original molecules for ROSs generation, for example ·OH from H_2O and $\cdot O_2^-$ from O_2, is also a very important factor for the utilization of excited electrons and holes.[11] Meanwhile, pollutants should be also properly adsorbed on the photocatalyst, and the generated ROSs should be utilized promptly due to their short life time to attack organic bonds in organic pollutants, i.e., the adsorption of pollutants on photocatalyst is also important to facilitate the interaction of ROSs and pollutants. Therefore, the evaluation procedure of photocatalyst's performance in DFT calculations are proposed in this work from the four aspects: (i) band structure of photocatalysts, including the band gap, the capability of photo adsorption and the positions of CB and VB; (ii) adsorption of H_2O, O_2 or other oxidants for the generation of ROSs; (iii) adsorption of pollutants; (iv) reaction pathway for pollutant degradation.

Graphitic carbon nitride (g-C_3N_4), a two dimensional (2D) non-metal semiconductor, has a lot of advantages as a photocatalyst, such as unique electronic properties, [21-24] high thermal conductivity,[10] porosity and large surface area, [25, 26] low cost [27] and easy to synthesis.[11] In addition, it is a green catalyst without any potential secondary contamination.[10, 11] However, the photocatalytic efficiency of pristine g-C_3N_4 is still not satisfactory due to the relatively large bandgap 3.02 eV and the high recombination rate of the photogenerated electron-hole pairs,[28, 29] limiting its visible-light absorption and utilization.[30,12] On the other hand, the energy level of valence band maximum (VBM) of g-C_3N_4 is at 1.4 V (vs. NHE at pH = 7), resulting in a weak oxidation ability (oxidative potential) to generate ·OH radicals.[31, 32] In 2014, Xie *et al.* studied the performance of g-C_3N_4 dots and found the UV-vis spectrum of g-C_3N_4 dots show an absorption band at 350 nm (band gap is 4.170 eV).[33] Wang *et al.* indicated that a wider band gap keeps a significant difference in the photophysical properties and photoexcited charge carriers for g-C_3N_4 dots to have excellent redox capability to generate both ·OH and $\cdot O_2^-$ radicals,[34] but the increase of band gap may inhibit the generation capacity of the electron-hole pairs.[30]

Creating heterostructure by using different semiconductors is an important way to improve the performance of photo-catalysts.[35] Yan *et al.* prepared polymer composites of carbon nitride and poly (3-hexylthiophene) with great photoabsorption performance, which inhibits the recombination of electron-hole pairs and improves photocatalytic activity.[36] Sun *et al.* synthesized the layered graphene/g-C_3N_4 composites with improved conductivity and electrocatalytic performance.[37, 38] WO_3/g-C_3N_4 and TiO_2/g-C_3N_4 were also studied for degradation of acetaldehyde and formaldehyde in VOCs.[39,40] Therefore, hetero-structure should be also a promising way to reduce the band gap of g-C_3N_4 dots and inhibit the recombination of electron-hole pairs, thus achieving excellent photocatalytic performance.

Considering the excellent potential of g-C_3N_4 dots on photocatalytic application and high electrical conductivity of graphene, which benefits the separation of electron-hole pairs, g-C_3N_4 dots/graphene photocatalytic system is proposed and taken as an example to demonstrate the application of the newly proposed evaluation procedure to predict the performance of photocatalysts based on DFT calculations. The band structure, optical properties, orbitals are calculated to understand the generation and recombination of electron-hole pairs. The calculations on work function, oxidation and reduction potential and adsorption to H_2O and O_2 are done to predict the generation efficacy of ·OH and $\cdot O_2^-$ radicals. In addition, the absorption performance of VOCs is also calculated to understand the possibility of degradation.

2. Calculation methods

All the calculations were performed based on DFT in this work,[41] and the band structure and photoadsorption spectrum calculations were implemented by CASTEP modulus, while DMOL3 modulus was adopted for the gas molecule absorption calculations.[23, 42] The exchange-correlation interactions were described by generalized gradient approximation (GGA) with the Perdew-Burke-Ernzerhof (PBE) functional.[43, 44] Spin-polarization was included in all calculations and a damped van der Waals correction was incorporated using Grimme's scheme to describe the non-bonding interactions.[45] 0.005 Ha smearing was used in the calculations. The Brillouin zone was sampled with the Monkhorst-Pack mesh with K-points of 6×6×1 grid in reciprocal space during electronic structure calculations. The HSE06 function was employed for band structure calculations, which is more accurate. [16]

The graphene single atomic layer used in our simulation is 5×5×1 supercell with a vacuum width of 23 Å along normal to layer direction, which ensures that the interaction between the layers in different supercell is negligible.[23, 30, 46] All atoms are allowed to relax in all energy calculations. The adsorption energy E_{ads} of VOCs molecules on adsorbent is defined as[21]

$$E_{ads} = E_{VOCs+adsorbent} - (E_{adsorbent} + E_{VOCs}) \quad (1)$$

where the subscripts VOCs+adsorbent, adsorbent, and VOCs denote the adsorbent with VOCs adsorbed, clean adsorbent, and the isolated VOCs molecules, respectively.

3. Results and discussion

g-C_3N_4 has two typical structures [47] as shown in Fig. S1. The g-C_3N_4 dots (*s-triazine* and *tri-s-triazine* g-C_3N_4 dots in Fig. S2) were built by using the minimum repeat unit of each structure, while the graphene layer with 5×5×1 supercell is used to avoid the interaction between g-C_3N_4 dots in different supercells. Thus, considering the different stacking types, four adsorption models of g-C_3N_4 dots on graphene (g-C_3N_4 dots/graphene) were built as shown in Fig. 1. The trizine-ring of two typical g-C_3N_4 dots overlapped with graphene in Fig. 1a and 1c, while it is malposed in Fig. 1b and 1d. After the structure relaxation, it is found that the interaction between g-C_3N_4 dot and graphene is van der Waals force and the structure in Fig. 1d has the strongest interface interaction energy as listed in Table S1. In addition, the configuration of g-C_3N_4 dots in graphene with a 10×10×1 supercell in Fig. S3 is considered to verify the size effect between g-C_3N_4 dots and graphene. Results from Fig. S4 and Text S1 show that the adsorption energies, bandgaps and optical adsorption spectrums of g-C_3N_4 dots in 5×5×1 and 10×10×1 graphene are consistent, indicating the little influence of the supercell size. Therefore, the configuration that *tri-s-triazine* g-C_3N_4 dots adsorption on graphene in Fig. 1d is adopted for the subsequent investigation on the photocatalytic performance for the potential application of VOCs photocatalytic degradation. The pristine *tri-s-triazine* g-C_3N_4 dots and *tri-s-triazine* g-C_3N_4 dots in g-C_3N_4 dots/graphene were respectively defined as p-CND and a-CND as show in Fig. S5(a) and S5(b).

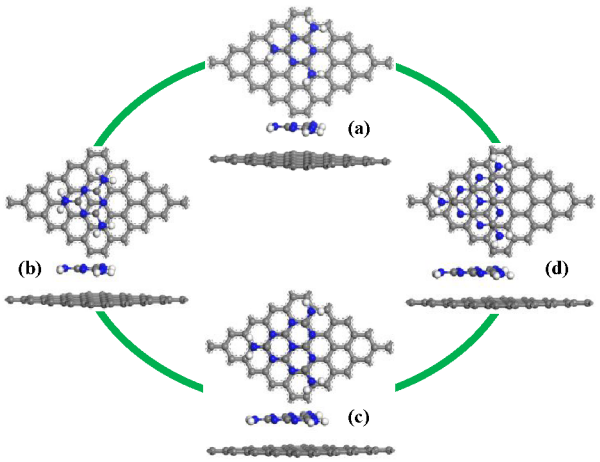

Fig. 1 The different optimized stacking configurations of g-C_3N_4 dots/graphene. Atom color code in this and following figures: carbon (grey), nitrogen (blue), hydrogen (white).

As introduced in the introduction section, photocatalytic performance of g-C_3N_4 dots/graphene system can be investigated from two aspects: band structure of g-C_3N_4 dots/graphene system for the evaluation of photo generation and recombination of electron-hole pairs, adsorption of H_2O/O_2 and VOCs on g-C_3N_4 dots/graphene system for the generation of ROSs and the subsequent utilization for VOCs degradation, which are investigated below in details.

3.1 Efficiency of electron-hole pairs generation and recombination

After the atomic configuration of g-C_3N_4 dots/graphene system was determined, the electronic structure of this system is calculated to understand the photo response properties. The band structures and density of states (DOS) of related materials are shown in Fig. 2. We can see that the band gaps of p-CND, g-C_3N_4 and graphene are respectively 4.454, 3.000 and 0 eV, which are consistent with the reported results of 4.170,[33] 3.020[16] and 0[45] eV. More interestingly, the band gap of the g-C_3N_4 dots/graphene composite is sharply reduced to 47 meV as shown in Fig. 2c, which indicates the promising conductivity of the g-C_3N_4 dots/graphene system.

To understand the effect of the interface interaction between a-CND and graphene, band structures of both g-C_3N_4 dots/graphene composite (gray dashed line) and pristine graphene (black line) are shown in Fig. 2d. It shows that the curves near the Fermi level are almost overlapped, which confirms the significant improvement of the composite conductivity due to the presence of graphene. In addition, the van der Waals interaction at the interface does not change the band structure of graphene much, which is indicated by the fact that the band curves of graphene in the composite almost overlap with those of pristine graphene, but the interface interaction opens a band gap of 47 meV for graphene in the composite. Besides, the VB and CB of g-C_3N_4 dots/graphene are mainly contributed by a-CND and graphene respectively, while the bands near the Fermi level are mainly contributed by graphene. Our results suggest that the photo excited electrons may transfer from the valence band of g-C_3N_4 dots directly into the band of graphene at Fermi level, following by migrating to the conduction band of g-C_3N_4 dots.

In addition, we also calculated the density of states (DOS) and partial density of states (PDOS) of each system to better understand the photocatalytic mechanism and the role of each component for the photocatalysis. The detailed results are shown in Fig. 2e and 2f. For Fig. 2e, the band gap of p-CND is obviously larger than that of g-C_3N_4, which is consistent with the band structure results. The a-CND band gap of 4.204 eV is slightly reduced relatively to p-CND, improving photocatalysis. Furthermore, near the Fermi level, both the a-CND and graphene contribute to the VB part, while only graphene locates on the CB part from Fig. 2f.

As described above, the photoadsorption performance of g-C_3N_4 is not ideal due to the limited visible light excitation [30] and weak oxidation ability.[31, 32] Therefore, the optical properties for p-CND, g-C_3N_4 and g-C_3N_4 dots/graphene were calculated in this work and the results are shown in Fig. 3. Note that the optical absorption spectrum, dielectric functions, dispersion curve and reflectance spectrum in our work are calculated by hybrid functional methods (HSE06) [48, 49] to obtain the more accurate results. As shown in Fig. 3a and 3b, g-C_3N_4 dots/graphene has remarkable visible light response as well as improved ultraviolet

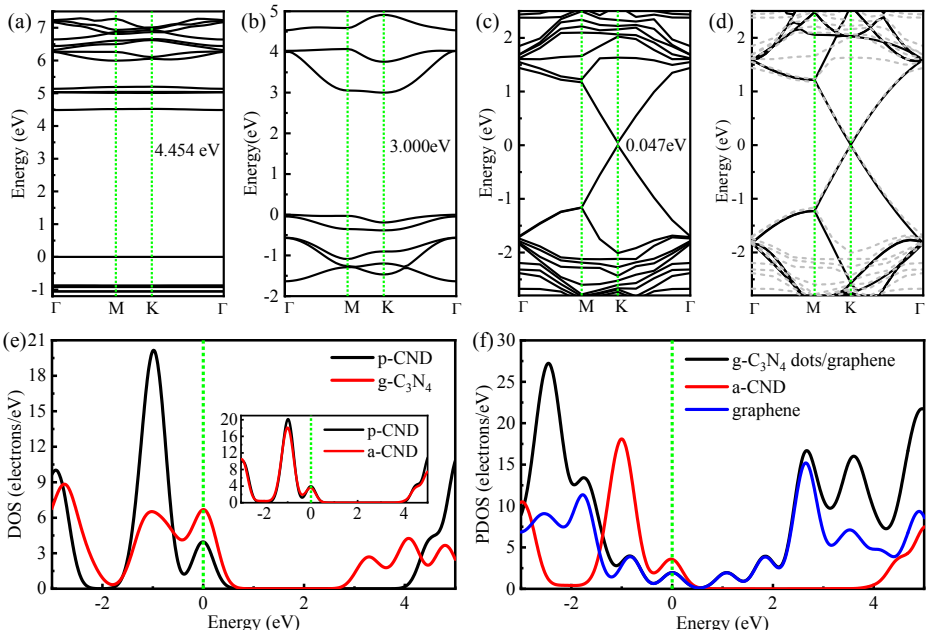

Fig. 2 The band structures of p-CND (a), g-C_3N_4 (b), g-C_3N_4 dots/graphene (c), graphene (d); the DOS and PDOS diagrams for several systems (e and f). The grad dashed line in (d) indicates the band structure of g-C_3N_4 dots/graphene.

(UV) response, whose energy is half of the sunlight energy. Meanwhile, the bulk g-C_3N_4 has weak visible light response and p-CND does not response under visible light response, but extending to the UV area due to the band gap increase when bulk g-C_3N_4 decreasing into dots. Therefore, the electron coupling at the g-C_3N_4 dots/graphene interface may induce a new optical transition and improve the visible light response property significantly, i.e. the g-C_3N_4 dots/graphene composite is expected to display obvious optical activity at the visible light range. In addition, p-CND and g-C_3N_4 can be excited at approximately 4.5 eV and 3 eV, which is also consistent with the results of corresponding band gaps of p-CND and g-C_3N_4. However, there is a noticeable adsorption peak at around 2 eV for the g-C_3N_4 dots/graphene system. This phenomenon shows that the graphene should be a bridge for the electron excitation from the VB of g-C_3N_4 dots to CB and the minimum energy of g-C_3N_4 dots/graphene photo-excitation can be reduced by nearly half, making the electron-hole pairs generation much easier. Therefore, the efficiency of electron excitation in the composite system can be greatly improved due to the reduced band gap and improved optical adsorption performance, especially under the visible light range. Noted that the energy of the adsorption peaks in UV range of g-C_3N_4, p-CND and g-C_3N_4 dots/graphene is in the order of g-C_3N_4 < p-CND < g-C_3N_4 dots/graphene as shown in Fig. 3b, which is consistent with the bandgap order g-C_3N_4 < p-CND < a-CND in Fig. 2. In other words, electrons can be also immigrated from the VB directly to CB of a-CND under UV irradiation.

In addition, the dielectric function is an important indicator for photoadsorption property. In general, the maximum imaginary part of the dielectric function indicates the maximum amount of photon adsorption.[50] As shown in Fig. 3c, the imaginary part in dielectric function of g-C_3N_4 and p-CND within the visible wavelength is gradually reduced to 0, while g-C_3N_4 dots/graphene has strong peak in the visible light range, and even higher peak at infrared ray (IR) range. Therefore, the composite system has a better photo absorption effect than those of p-CND and g-C_3N_4, enhancing the utilization of visible light and IR and improving the yield of the photo generated electron-hole pairs. We also calculated the dispersion curve that is the relationship between refractive index and wavelength, shown as the black curve in Fig. 3d. The refractive index is the rate of the spread of light on vacuum conduction to that on other materials, and it is an important parameter for materials to apply as optoelectronic devices.[51] Therefore, refractive index must be bigger than 1 because the spread of light on vacuum conduction is maximum. It can be found that refractive index of g-C_3N_4 dots/graphene reaches to its maximum in the infrared range, whereas the minimum has been achieved in UV range. In addition, the refractive index of g-C_3N_4 dots/graphene is more than 1 in entire infrared region and partial visible and UV region. Thus, in the visible region of 2.30 eV~3.11 eV (about 399 nm~540 nm), the g-C_3N_4 dots/graphene can refract light and shows a good photocatalytic performance. According to the red line of reflectance spectrum, g-C_3N_4 dots/graphene has a reflection peak in the infrared and UV regions, while a trough in the visible area. Those phenomenon in dispersion curve and reflectance spectrum are advantageous to the transfer of light in the material and beneficial to photocatalysis.

Another important factor limiting photocatalytic applications in g-C_3N_4 is the massive electron-hole recombination rate.[12]

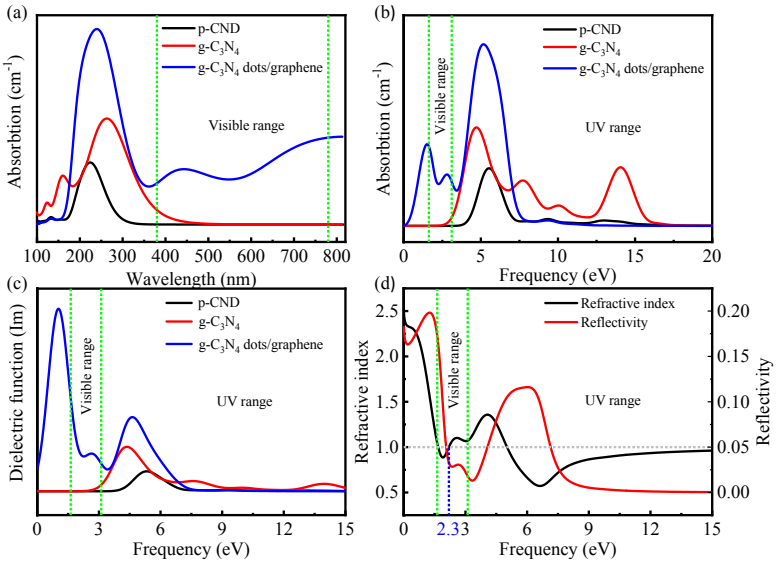

Fig. 3 Optical adsorption behaviors of p-CND, g-C_3N_4 and g-C_3N_4 dots/graphene with wavelength of nm (a) and frequency of eV (b); the imaginary parts of several dielectric functions (c); the dispersion curve (black) and reflectance spectrum (red) of g-C_3N_4 dots/graphene (d).

Thus, the orbital (HOMO-LUMO) of g-C_3N_4 dots/graphene was calculated by using DMOL3 modulus to explore the electron excitation pathway. HOMO is the electron distribution of the highest occupied molecular orbital, which corresponding to the curve of valence band maximum (VBM) in band structure as shown in Fig. 2, while LUMO is the electron distribution of the lowest unoccupied molecular orbital, corresponding to the curve of conductive band minimum (CBM). In other words, HOMO and LUMO are electron distribution states before and after the photo excitation. Fig. 4a is the HOMO and LUMO of g-C_3N_4. It shows that the HOMO localizes all on the N atoms, while the LUMO mainly distributes on C atoms and partly on N atoms. However, no electrons would be excited from bridging N atoms under light irradiation, and the photogenerated electrons neither migrate to bridging N atoms nor transfer from one heptazine (C_6N_7) unit to the adjacent unit through bridging N atoms. This means that the excited electron-hole pairs are localized in each triazine unit, and indicating high electron-hole recombination possibility, which worsens the photocatalytic efficiency. This conclusion is also consistent with the reported DFT result.[52]

However, Fig. 4b clearly shows the HOMO in g-C_3N_4 dots/graphene locates on N atoms of the g-C_3N_4 dot, while the LUMO distributes on the graphene, which suggests that electrons are directly excited from the g-C_3N_4 dot to graphene for the photo excitation, separating electrons and holes. In addition, graphene has excellent conductivity to transfer the excited electrons away, further preventing the generated electron-hole recombination. Combining the analyses of band structures, optical property and HOMO-LUMO orbitals in Figs. 2-4, the electron photo excitation path in g-C_3N_4 dots/graphene is from the VB of g-C_3N_4 dots, to the band at the Fermi level of graphene, and then to the CB of g-C_3N_4 dots. The energy required for the electron excitation in g-C_3N_4 dots/graphene system is half of that in g-C_3N_4 dots, which would facilitate the generation of electron-hole pairs dramatically. Meanwhile, g-C_3N_4 dots/graphene system has lower recombination rate because the excited electron and holes are respectively in graphene and g-C_3N_4 dots. In other words, g-C_3N_4 dots/graphene system can be easily photo excited and the electrons and holes can be utilized effectively for photocatalysis.

To better analyze the related influencing factors on g-C_3N_4 dots/graphene to photocatalytically degrade VOCs, elemental PDOS in different systems were also calculated. For g-C_3N_4 system (Fig. 5a), the VB is mainly dominated by N atoms, while the CB is contributed by both C and N atoms. This conclusion is consistent with the HOMO-LUMO results in Fig. 4a. In addition, the VB and CB of p-CND in Fig. 5b is similar with that of g-C_3N_4 except the effect of H atoms, which are not included in pristine g-C_3N_4. However, we can see from Fig. 5c that the C and N atoms play a significant role in VB of g-C_3N_4 dots/graphene, while C, N, H atoms are all of the same importance in CB part.

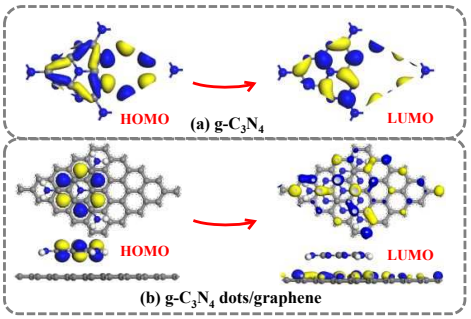

Fig.4 The HOMO-LUMO orbitals of g-C_3N_4 (a) and g-C_3N_4 dots/graphene (b).

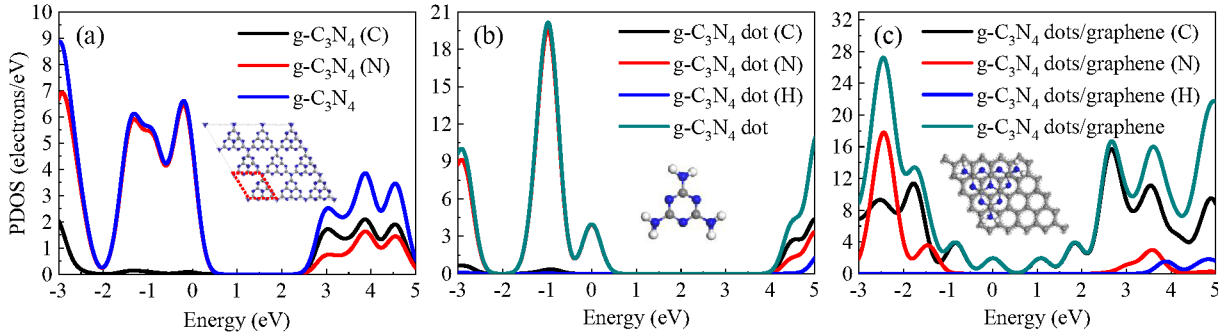

Fig. 5 The partial density of states (PDOS) of different elements for g-C_3N_4 (a), g-C_3N_4 dot (b) and g-C_3N_4 dots/graphene (c)

3.2 The adsorption of various VOCs

The g-C_3N_4 dots/graphene acts as a catalyst to play a significant effect only on its excellent performance to capture VOCs. Thus, the factor of VOCs adsorption is considered. There are different types of VOCs, such as alkanes, olefins, alcohols, ketones, aldehydes, aromatics, halogenated hydrocarbons, etc. Among them, the most common and toxic compounds are formaldehyde, benzene, toluene, propylene, phenol, acetone, and styrene.[1, 2, 41] Moreover, trichloroethylene (TCE) as an organochloride compound in gas phase is high toxicity and results in serious environmental and human health problems.[53, 54] Hence, the five typical VOCs gases, benzene, toluene, formaldehyde, styrene and TCE, were chosen as examples to study the universality of g-C_3N_4 dots/graphene in adsorption performance for VOCs gases. Then the adsorption of the five VOCs molecules on pristine g-C_3N_4 and graphene were also investigated, respectively. Through the DFT calculations on all the possible adsorption configurations and considering both horizontal and vertical directions, adsorption energy (E_{ads}) of the most stable configuration of individual VOCs on different adsorbent is listed in Table 1. The corresponding configurations are shown in Table S2.

Table 1 Adsorption energy of VOCs on g-C_3N_4, graphene and g-C_3N_4 dots/graphene

	Benzene (eV)	Toluene (eV)	Formaldehyde (eV)	Styrene (eV)	TCE (eV)
CN	-0.568	-0.696	-0.531	-0.712	-0.610
G	-0.655	-0.738	-0.317	-0.806	-0.745
CNG	-0.920	-1.120	-0.872	-1.264	-1.090

CN: g-C_3N_4; G: grapheme; CNG: g-C_3N_4 dots/graphene

The adsorption energy values of benzene, toluene, formaldehyde, styrene and TCE on g-C_3N_4 dots/graphene system are -0.920, -1.120, -0.872, -1.264 and -1.090 eV, respectively. Compared with that on g-C_3N_4 and graphene, adsorption energy of the five VOCs molecules on g-C_3N_4 dots/graphene is increased significantly. It is considered that the combination of graphene and g-C_3N_4 has a significant effect on the enhanced adsorption of VOCs. In addition, this phenomenon also indicates g-C_3N_4 dots/graphene as a photocatalyst can be widely applied in most VOCs. The good adsorption property of g-C_3N_4 dots/graphene provides a promising precondition for the photocatalytic degradation of VOCs.

3.3 The formation of $\cdot O_2^-$ and ·OH radicals

As described in the introduction section, the adsorption of H_2O and O_2 molecules is also essential in photocatalysis for the generation of hydroxyl (·OH) and superoxide ($\cdot O_2^-$) radicals to degrade pollutants. Ji *et al.*[55] reassessed the effect of ·OH to toluene; Yu et al.[40] reported the relationship between ·OH and formaldehyde; Chen *et al.*[56] indicated ·OH determines photocatalytic degradation mechanisms of styrene; Gu *et al.*[54] shown the importance of ·OH and $\cdot O_2^-$ to TCE. In addition, the significant function of two free radicals had been exposed by other researchers.[39, 57] Therefore, the adsorption of H_2O and O_2 molecules on g-C_3N_4, graphene and g-C_3N_4 dots/graphene were calculated with considering all possible adsorption sites and orientations. After DFT calculations, the optimal configuration as well as the corresponding adsorption energy are summarized in Table S3 and Table 2. The adsorption energies of H_2O on g-C_3N_4, graphene and g-C_3N_4 dots/graphene are obtained as -0.692, -0.328, -0.849 eV, respectively (g-C_3N_4 dots/graphene > g-C_3N_4 > graphene), which shows that the adsorption energy of H_2O on the composite of g-C_3N_4 dots/graphene is significantly enhanced. Similarly, the O_2 adsorption energy of 1.720 eV on g-C_3N_4 dots/graphene is also superior to others of g-C_3N_4 and graphene. These results provide a prerequisite for the generation of hydroxyl (·OH) and superoxide ($\cdot O_2^-$) radicals.

Table 2 The adsorption energy of g-C_3N_4, graphene and g-C_3N_4 dots/graphene to absorb H_2O and O_2 molecules, respectively

	g-C_3N_4 (eV)	graphene (eV)	g-C_3N_4 dots/graphene (eV)
H_2O	-0.692	-0.328	-0.849
O_2	-1.533	-1.630	-1.720

In addition, a suitable band edge positions to produce $\cdot O_2^-$ and ·OH radicals are crucially important for a photocatalyst for VOCs photodegradation. To determine the thermodynamic ability of these systems to generate the $\cdot O_2^-$ and ·OH, the work function method[52, 58, 59] calculated by HSE06 function on CASTEP model was used to determine the corresponding valence band

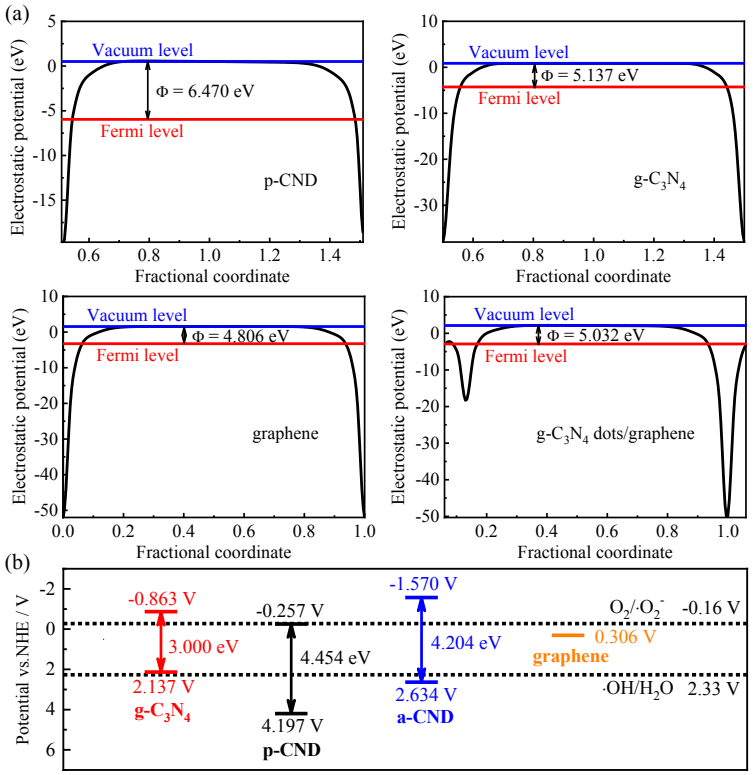

Fig. 6 Work functions for p-CND, g-C_3N_4, graphene and g-C_3N_4 dots/graphene (a); band edge position and oxidation reduction potential of several systems for $O_2/{\cdot}O_2^-$ and ${\cdot}OH/H_2O$ potential (b).

maximum (VBM) and conduction band minimum (CBM) edge positions of g-C_3N_4, p-CND and a-CND based on the following equations.

$$E_{VBM}(\text{eV}) = -\Phi + 0.5E_g \quad (2)$$

$$E_{CBM}(\text{eV}) = -\Phi - 0.5E_g \quad (3)$$

$$E'_{CBM/VBM}(\text{V}) = -E_{VBM/CBM}(pH = 7) - 4.5 \quad (4)$$

where Φ is work function, E_g is band gap, and $E'_{CBM/VBM}$ is potential versus NHE (pH = 7, 0 V vs. NHE ~ -4.5 eV). The work functions of p-CND, g-C_3N_4, graphene and g-C_3N_4 dots/graphene are 6.470, 5.137, 4.806 and 5.032 eV, respectively (Fig. 6a). Fig. 2 shows that the band gaps of g-C_3N_4, p-CND, graphene and a-CND are respectively 3.000, 4.454, 0 and 4.204 eV, while the reported chemical potential values for corresponding free radical generation are shown in the following:[60]

$$E^0(O_2/{\cdot}O_2^-) = -0.16 \text{ V vs. NHE}$$

$$E^0({\cdot}OH/H_2O) = 2.33 \text{ V vs. NHE}$$

According to the above formula, the CBM and VBM of different systems and relevant oxidation reduction potential are shown in Fig. 6b. As shown in Fig. 6b, the CBM of g-C_3N_4, p-CND and a-CND are respectively -0.863, -0.257 and -1.570 V, which are above the redox potential of $O_2/{\cdot}O_2^-$ of -0.16 V. The result shows that all the three systems could generate ${\cdot}O_2^-$, and the efficiency of g-C_3N_4 dots/graphene is higher than that of g-C_3N_4 and pristine g-C_3N_4 dots. The VBM of p-CND and a-CND are respectively 4.197 and 2.634 V, higher than the ${\cdot}OH/H_2O$ chemical potential of 2.33 V, but the VBM of g-C_3N_4 is 2.137 V, lower than the ${\cdot}OH/H_2O$ chemical potential of 2.33 V. Therefore, g-C_3N_4 can only photoactivate O_2 into ${\cdot}O_2^-$, while the ability to generate ${\cdot}OH$ radical is weak. This is also consistent with reported result that g-C_3N_4 has a weak oxidative potential to produce ${\cdot}OH$ radical.[31] For p-CND and a-CND, the both reactions of H_2O to ${\cdot}OH$ and O_2 to ${\cdot}O_2^-$ can proceed. Noted that the CBM of a-CND is more negative than the edge position of p-CND (a-CND: -1.570 V; p-CND: -0.257 V), and the VBM is more thermodynamically favorable than the reduction potential of ${\cdot}OH/H_2O$. Thus, the both photoelectrochemical process ($O_2/{\cdot}O_2^-$ and ${\cdot}OH/H_2O$) could occur in the system of g-C_3N_4 dots/graphene or pristine g-C_3N_4 dots once the electron-hole pairs are photoactivated. However, the band gaps of g-C_3N_4 dots are 4.454 eV (p-CND) and 4.204 eV (a-CND), which is too large for visible light activation. The presence of graphene in g-C_3N_4 dots/graphene system can significantly reduce the photo activation energy, which will be explained in details in the section of photo activation mechanism. In addition, the spin density in Fig. S6 also directly confirms the generation of free radicals with lone pair electrons.

3.4 The photocatalytic degradation mechanism of VOCs on g-C_3N_4 dots/graphene

To better illustrate the mechanism of electron transfer and VOCs degradation, a scheme for the corresponding photocatalytic mechanism of the g-C_3N_4 dots/graphene system is shown in Fig. 7. For photo activation process, once the photo irradiation energy is higher than the excitation energy of nanostructured photocatalysts, photo excitation occurs with the generation of electron-hole pairs, where the electrons in the valence band jump to the conductive band and holes remain in the valence band.[30, 61] For the g-C_3N_4 dots/graphene system, graphene has a tiny band gap of 47 meV and the corresponding CBM and VBM positions are also shown in Fig. 6b. In addition, the photoactivated electrons are from g-C_3N_4 dots to graphene from Figs. 4b and 6b, i.e. the photo activation is consistent by two steps: the electrons in valence band of g-C_3N_4 dots first jump to the band of graphene, which is located close to the Fermi level; then the electrons can continue to jump to the conductive band of g-C_3N_4 dots. The energy gap for each step is ~2 eV, which can be easily provided by visible light and even IR. This pathway can be confirmed by strong visible light adsorption ~2.5 eV, almost half of the energy of adsorption peak ~5 eV for g-C_3N_4 and p-CND as shown in Fig. 3b. In addition, as shown in Fig. 6b, the activated electrons and holes have strong capability to active both H_2O and O_2 molecules in air to effectively generate $\cdot O_2^-$ and ·OH radicals, which can be used for VOCs degradation on the surface of photocatalysts. Fig. S7 is an example of the reaction pathway for formaldehyde degradation in the presence of ·OH and $\cdot O_2^-$ radicals. The corresponding explanation was described in Text S2. Besides the efficient generation of electron-hole pairs, the recombination of the generated electron-hole pairs can be also effectively restrained due to the separation of electron and hole respectively on graphene and g-C_3N_4 dots, and the electrons on graphene can be also transported to elsewhere due to the high conductivity of graphene.

This work aims to propose the evaluation procedure of photocatalysis from the view of DFT calculation, and confirm the effectiveness of this procedure by taking an example. For the chemical criteria, many researchers have indicated possible pathways of VOCs degradation by ·OH and $\cdot O_2^-$ radicals.[54-56] Hence, the reaction pathway of free radicals to degrade VOCs on the surface of catalysts was not calculated in this work, which will be discussed in detailed in our following work.

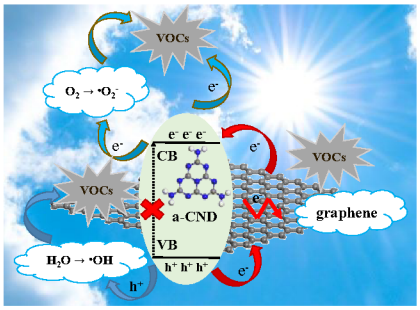

Fig. 7 The mechanism of electron transfer and VOCs degradation under visible light irradiation.

4. Conclusion

In this work, the evaluation procedure of the performance of photocatalysts from the view of density functional theory calculation was proposed: band structure of photocatalysts, including the band gap, the capability of photo adsorption and the positions of CB and VB; adsorption of H_2O, O_2 or other oxidants; adsorption of pollutants; reaction pathway of pollutant degradation. The g-C_3N_4 dots/graphene is taken as an example to demonstrate the application of the newly proposed evaluation procedure. We found that the g-C_3N_4 dots/graphene composite is an excellent photocatalyst based on following aspects: (i) Compared with g-C_3N_4 and g-C_3N_4 dots, the band gap and photo adsorption of g-C_3N_4 dots/graphene are more suitable, which are more prone to light excitation and generate electron-hole pairs; (ii) The g-C_3N_4 dots/graphene has lower electron recombination rate for perfect photocatalytic degradation with photoelectron being excited between the heterostructure from g-C_3N_4 dots to graphene layer, which prevents the recombination of electron-hole pairs, while electron migration in g-C_3N_4 is localized within each C_6N_7 unit; (iii) H_2O, O_2 and VOCs can be well adsorbed on g-C_3N_4 dots/graphene, effectively producing corresponding free radicals (·OH, $\cdot O_2^-$) to degrade VOCs due to the suitable CB and VB positions; (iv) Most importantly, a new electronic migration path of g-C_3N_4 dots/graphene is demonstrated from the valence band of g-C_3N_4 dots, leap to graphene, and then to the conduction band of g-C_3N_4 dots. This pathway could reduce nearly half of energy required for electronic excitation and is beneficial to photocatalysis under visible light and even IR light. Therefore, the evaluation procedure of high-performance photocatalysts based on DFT calculations is proposed systematically, which is adopted to guide and design high-performance photocatalyst g-C_3N_4 dots/graphene for VOCs degradation.

Conflicts of interest

There are no conflicts to declare.

Acknowledgements

This work was supported by the National Natural Science Foundation of China (no. 21607029, 21777033, 41425015), Science and Technology Planning Project of Guangdong Province (2017B020216003).

Notes and references

1. S. Scirè and L. F. Liotta, *Applied Catalysis B: Environmental*, 2012, **125**, 222-246.
2. L. F. Liotta, *Applied Catalysis B: Environmental*, 2010, **100**, 403-412.
3. A. G. Carlton, C.Wiedinmyer and J. H. Kroll, *Atmospheric Chemistry and Physics*, 2009, **8**, 4987-5005.
4. M. Amann and M. Lutz, *Journal of Hazardous Materials*, 2000, **78**, 41-62.

5. B. Liu, W. Zhao, Q. Jiang, Z. Ao and T. An, *Sustainable Materials and Technologies*, 2019, **21**, e00103.
6. W. P. L. Carter, *Journal of the Air & Waste Management association*, 1994, **44**, 881-899.
7. Y. Su, Z. Ao, Y. Ji, G. Li and T. An, *Applied Surface Science*, 2018, **450**, 484-491.
8. Z. Ao, H. Sun and A. Fullana, *Frontiers in Chemistry*, 2019, **7**, 75.
9. Y. Yang, M. Wu, X. Zhu, H. Xu and J. Ma, *Chinese Chemical Letters*, 2019, **30**, 2065-2088.
10. X. Duan, Z. Ao, H. Sun, S. Indrawirawan, Y. Wang, J. Kang, F. Liang, Z. H. Zhu and S. Wang, *ACS Applied Materials & Interfaces*, 2015, **7**, 4169-4178.
11. M. Wu, X. He, B. Jing, T. Wang, C. Wang, Y. Qin, Z. Ao, S. Wang and T. An, *Journal of Hazardous Materials*, 2020, **384**, 121323.
12. M. Wu, H. Lv, T. Wang, Z. Ao, H. Sun, C. Wang, T. An and S. Wang, *Catalysis Today*, 2018, **315**, 205-212.
13. K. Dai, L. Lu, Q. Liu, G. Zhu, X. Wei, J. Bai, L. Xuan and H. Wang, *Dalton Transactions*, 2014, **43**, 6295-6299.
14. X. Ye, S. Ma, X. Jiang, Z. Yang, W. Jiang and H. Wang, *Chinese Chemical Letters*, 2019, **30**, 2123-2131.
15. C. Nie, Z. Dai, H. Meng, X. Duan, Y. Qin, Y. Zhou, Z. Ao, S. Wang and T. An, *Water Research*, 2019, **166**, 115043.
16. G. Gao, Y. Jiao, F. Ma, Y. Jiao, E. Waclawik and A. Du, *Physical Chemistry Chemical Physics*, 2015, **17**, 31140-31144.
17. J. Zhou, G. Liu, Q. Jiang, W. Zhao, Z. Ao and T. An, *Chinese Journal of Catalysis*, 2020, **41**, 1633-1644.
18. L. Zhou, H. Zhang, H. Sun, S. Liu, M. O. Tade, S. Wang and W. Jin, *Catalysis Science & Technology*, 2016, **6**, 7002-7023.
19. A. Ajmal, I. Majeed, R. N. Malik, H. Idriss and M. A. Nadeem, *RSC Advances*, 2014, **4**, 37003-37026.
20. M. Lei, N. Wang, L. Zhu, Q. Zhou, G. Nie and H. Tang, *Applied Catalysis B: Environmental*, 2016, **182**, 414-423.
21. Z. M. Ao, Q. Jiang, R. Q. Zhang, T. T. Tan and S. Li, *Journal of Applied Physics*, 2009, **105**, 074307.
22. M. Zhou, Y. H. Lu, Y. Q. Cai, C. Zhang and Y. P. Feng, *Nanotechnology*, 2011, **22**, 385502.
23. Z. M. Ao, J. Yang, S. Li and Q. Jiang, *Chemical Physics Letters*, 2008, **461**, 276-279.
24. F. Schedin, A. K. Geim, S. V. Morozov, E. W. Hill, P. Blake, M. I. Katsnelson and K. S. Novoselov, *Nature Materials*, 2007, **6**, 652-655.
25. Y. Zheng, J. Liu, J. Liang, M. Jaroniec and S. Z. Qiao, *Energy Environmental Science*, 2012, **5**, 6717-6731.
26. Y. Wang, X. Wang and M. Antonietti, *Angewandte Chemie International Edition*, 2012, **51**, 68-89.
27. Y. Wu, Q. Chen, S. Liu, H. Xiao, M. Zhang and X. Zhang, *Chinese Chemical Letters*, 2019, **30**, 2186-2190.
28. W. Liu, Y. Li, F. Liu, W. Jiang, D. Zhang and J. Liang, *Water Research*, 2019, **151**, 8-19.
29. H. Ji, P. Du, D. Zhao, S. Li, F. Sun, E. C. Duin and W. Liu, *Applied Catalysis B: Environmental*, 2020, **263**, 118357.
30. B. Jing, Z. Ao, Z. Teng, C. Wang, J. Yi and T. An, *Sustainable Materials and Technologies*, 2018, **16**, 12-22.
31. H. Sun, G. Zhou, Y. Wang, A. Suvorova and S. Wang, *ACS Applied Materials Interfaces*, 2014, **6**, 16745-16754.
32. G. Liu, P. Niu, C. Sun, S. C. Smith, Z. Chen, G. Q. M. Lu and H.-M. Cheng, *Journal of American Chemical Society*, 2010, **132**, 11642-11648.
33. X. Zhang, H. Wang, H. Wang, Q. Zhang, J. Xie, Y. Tian, J. Wang and Y. Xie, *Advanced Materials*, 2014, **26**, 4438-4443.
34. T. Wang, C. Nie, Z. Ao, S. Wang and T. An, *Journal of Materials Chemistry A*, 2020, **8**, 485-502.
35. P. Niu, L. Zhang, G. Liu and H. M. Cheng, *Advanced Functional Materials*, 2012, **22**, 4763-4770.
36. H. Yan and Y. Huang, *Chemical Communications*, 2011, **47**, 4168-4170.
37. Q. Xiang, J. Yu and M. Jaroniec, *Journal of Physical Chemistry C*, 2011, **115**, 7355-7363.
38. Y. Sun, C. Li, Y. Xu, H. Bai, Z. Yao and G. Shi, *Chemical Communication*, 2010, **46**, 4740-4742.
39. K. Katsumata, R. Motoyoshi, N. Matsushita and K. Okada, *Journal of Hazardous Materials*, 2013, **260**, 475-482.
40. J. Yu, S. Wang, J. Low and W. Xiao, *Physical Chemistry Chemical Physics*, 2013, **15**, 16883-16890.
41. G. Liu, J. Zhou, W. Zhao, Z. Ao and T. An, *Chinese Chemical Letters*, 2020, DOI: 10.1016/j.cclet.2019.12.023.
42. B. Delley, *Journal of Chemical Physics*, 2000, **113**, 7756-7764.
43. T. Liao, C. Sun, A. Du, Z. Sun, D. Hulicova-Jurcakova and S. Smith, *Journal of Materials Chemistry*, 2012, **22**, 8321-8326.
44. J. P. Perdew, K. Burke and M. Ernzerhof, *Physical Review Letters*, 1996, **77**, 3865-3868.
45. A. Du, S. Sanvito, Z. Li, D. Wang, Y. Jiao, T. Liao, Q. Sun, Y. H. Ng, Z. Zhu, R. Amal and S. C. Smith, *Journal of the American Chemical Society*, 2012, **134**, 4393-4397.
46. B. T. Teng, F. M. Wu, W. X. Huang, X. D. Wen, L. H. Zhao and M. F. Luo, *Chemphyschem*, 2012, **13**, 1261-1271.
47. L. Liu, H. Lv, C. Wang, Z. Ao and G. Wang, *Electrochim Acta*, 2016, **206**, 259-269.
48. L. Ruan, G. Xu, L. Gu, C. Li, Y. Zhu and Y. Lu, *Materials Research Bulletin*, 2015, **66**, 156-162.
49. J. Cui, S. Liang, X. Wang and J. M. Zhang, *Physical Chemistry Chemical Physics*, 2015, **17**, 23613-23618.
50. L. Sohrabi, A. Boochani, S. Ali Sebt and S. Mohammad Elahi, *The European Physical Journal Plus*, 2018, **133**, 117-129.
51. B. Yao, X. Hu, J. Liu, K. Chen and J. Liu, *Materials Letters*, 2020, **261**, 126878.
52. Y. Wang, Y. Tian, L. Yan and Z. Su, *The Journal of Physical Chemistry C*, 2018, **122**, 7712-7719.
53. I. Jansson, S. Suárez, F. J. Garcia-Garcia and B. Sánchez, *Applied Catalysis B: Environmental*, 2015, **178**, 100-107.
54. M. Gu, U. Farooq, S. Lu, X. Zhang, Z. Qiu and Q. Sui, *Journal of Hazardous Materials*, 2018, **349**, 35-44.
55. Y. Ji, J. Zhao, H. Terazono, K. Misawa, N. P. Levitt, Y. Li, Y. Lin, J. Peng, Y. Wang, L. Duan, B. Pan, F. Zhang, X. Feng, T. An, W. Marrero-Ortiz, J. Secrest, A. L. Zhang, K. Shibuya, M. J. Molina and R. Zhang, *Proceedings of the National Academy of Sciences of the United States of America*, 2017, **114**, 8169–8174.
56. J. Chen, Z. He, Y. Ji, G. Li, T. An and W. Choi, *Applied Catalysis B: Environmental*, 2019, **257**, 117912.
57. G. Mamba and A. K. Mishra, *Applied Catalysis B: Environmental*, 2016, **198**, 347-377.
58. D. K. Kanan and E. A. Carter, *The Journal of Physical Chemistry C*, 2012, **116**, 9876-9887.
59. F. Opoku, K. K. Govender, C. G. C. E. v. Sittert and P. P. Govender, *Applied Surface Science*, 2018, **427**, 487-498.
60. Q. Zheng, D. P. Durkin, J. E. Elenewski, Y. Sun, N. A. Banek, L. Hua, H. Chen, M. J. Wagner, W. Zhang and D. Shuai, *Environmental Science Technology*, 2016, **50**, 12938-12948.
61. X. Wang, K. Maeda, A. Thomas, K. Takanabe, G. Xin, J. M. Carlsson, K. Domen and M. Antonietti, *Nature Materials*, 2009, **8**, 76-80.

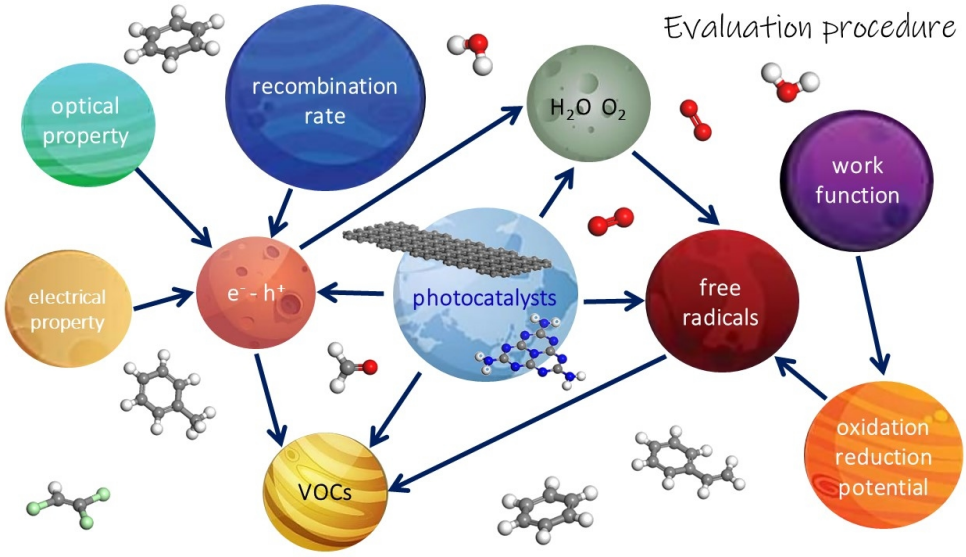

338x190mm (96 x 96 DPI)